FATIGUE DESIGN MODEL BASED ON DAMAGE MECHANISMS REVEALED BY ACOUSTIC EMISSION MEASUREMENTS

ICAS-94-9.1.1

D. Fang* and A. Berkovits**
*Post-Doctorate Fellow, Faculty of Eng., Tel Aviv University, Tel Aviv
**Assoc. Prof., Faculty of Aerospace Eng.
Technion - Israel Institute of Technology
Haifa 32000, Israel.

Abstract

Computerization of acoustic emission instrumentation has made AE monitoring of fatigue tests a practical possibiity. On-line processing provides a selection of software tools, enhancing classical techniques for eliminating the background noise which usually blanked out data. Fatigue tests monitored for acoustic emission were carried out at room temperature on Incoloy 901 material specimens, over a stress-ratio range of $-1 \le R \le 2$. Valid AE data were obtained even when the load cycle passed through zero. The AE data permitted identification of the various phenomena occurring on the way to final failure. These included initial plasticity, crack nucleation and propagation phases.The AE findings were supported by microscopic examination. Based on the experimental data, a damage-prediction model was formulated.

Nomenclature

K_{th}	=	threshold stress intensity factor
n	=	cycle count
N	=	fatigue lifetime
N_t	=	transition life
R	=	stress ratio, $\sigma_{min}/\sigma_{max}$
δ_i	=	material constants
ε	=	strain
ε_{max}	=	strain at σ_{max}
e_0	=	strain to initiate AE activity
η, η_i	=	ringdown counts; counts in stage
η_f	=	ringdown counts to failure
$\Delta\sigma$	=	stress range
σ_a, σ_m	=	stress amplitude, mean stress
$\sigma_{max}, \sigma_{min}$	=	maximum, minimum cyclic stress
σ_{op}	=	crack-opening stress
σ_{uts}	=	material strength
ϕ_i	=	load function
$\omega; \omega_1$	=	damage parameter η/η_f; first cycle damage

Other symbols are empirical constants.

Introduction

Acoustic emission (AE) has developed as a nondestructive evaluation technique and as a tool in materials research. It is a highly sensitive technique for detecting active microscopic processes in a material, as well as crack propagation. Because such events give rise to elastic waves which propagate through the material, passive AE monitoring to detect and locate the sonic source can inspect damage by using remote sensors, rather than requiring complete volumetric scanning [1-4].

The usefulness of AE testing has been considerably enhanced in recent years by the incorporation of the microcomputer into the AE instrumentation. Not only has the computer revolutionized the acquisition, recording and analysis of the large amount of data arising from an AE study. Above all, when combined with careful mechanical procedures, the computer has succeeded in containing the problem of background noise inherent in acoustic emission data emanating from the fatigue test.

Fatigue crack formation and initiation are preceded by progressive material deterioration, induced by dislocation motion and saturation, and a loss of resistance in terms of life. If it were possible to monitor this deterioration in real time, the measured quantities could be used as indicators of the extent of fatigue damage. Attention was focused in this investigation on the significance of acoustic emission as a measure of dislocation dynamics as well as crack growth in relation to the stress state.

In the paper, acoustic emission techniques developed for study of fatigue damage in Incoloy 901 superalloy are briefly described. After a discussion of AE characteristics the paper presents and discusses room temperature tests and results. Baseline tests included monotonic strength, and both strain- and stress-controlled fatigue tests over strain ratios $-1 \le R_\varepsilon \le 0.6$ and stress ratios $-1 \le R_\sigma \le 0.2$.

Fatigue tests monitored for acoustic emission were carried out over a stress-ratio range of $-1 \le R_\sigma \le 0.2$. Valid AE data were obtained even when the load cycle passed through zero. The AE data permitted correlation with the various phenomena occurring on the way to final failure. These included dislocation multiplication and saturation; initial plastic yielding, strain-hardening, and cyclic softening; crack incubation, and the instant of

crack initiation; fatigue crack propagation, and failure. Based on the experimental data, a preliminary damage-prediction model was formulated.

Characteristics of Acoustic Emission Signals

Acoustic emission results from the rapid release of energy from localized sources within a material[5]. In passive acoustic emission, the AE sensor locates and measures sound produced by a test object during deformation. The test object must be releasing energy, for example while being stressed or heated. Materials undergoing deformation may emit acoustic energy, usually in the form of short bursts or trains of fast impulses in the 100 kHz frequency range. When picked up by acoustic transducers these transient elastic wave signals can be related to the physical integrity of the material or structure in which they were generated. Monitoring of these events permits detection and location of flaws as well as prediction of impending failure. The advantages and drawbacks of AE testing are listed in Table 1.

Table 1. Characteristics of AE testing.

Advantages	**Drawbacks**
Real time evaluation	Discrimination between
Passive technique	noise and AE signals
Continuous monitoring	Requires experience and
High sensitivity	skill
Whole structure	Material behavior must
interrogation	be understood
Source location	Quantitative correlation
Active defects detected	limited at present
Pattern recognition	Passive defects not
aids interpretation	detected

Acoustic emission signals are generally described as burst or continuous-type emission (see Fig. 1), although what appears to be continuous emission in reality consists of bursts which are too small to be individually resolved. Continuous emission signals originate from such sources as leaks in pressurized systems, yielding in metals, hydraulic noise, and rotating machinery. Burst-type emission signals originate from sources such as intermittent dislocation motion and crack growth in metals, composites and geological materials as well as metal fretting and impact. The rise-rate and exponential decay of the burst wave is determined by the nature of the signal source, structural attenuation, wave-mode conversion between source and sensor, and the characteristic response of the sensor to the wave mode type.

Acoustic emission expected in fatigue studies is primarily of the burst type, from dislocation dynamics and crack growth in the material. The various parameters of an AE burst (Fig. 1) can be divided into: specific parameters, such as number of bursts or "events", ringdown counts per event, and peak amplitude; and global parameters, including event duration, rise time and rise rate, and event energy. Before reliable AE data can be obtained, however, significant background noise has to be overcome.

Software Techniques for Minimizing Background Noise

Studies of acoustic emission either on smooth specimens or in high-cycle fatigue have been few, primarily because of difficulties in eliminating extraneous background noise. Background noise is particularly serious in fatigue for two reasons. The AE signal level in fatigue is relatively low, while the cyclic-loading process is inherently noisy. Noise rejection methods in cyclic tests on smooth specimens include

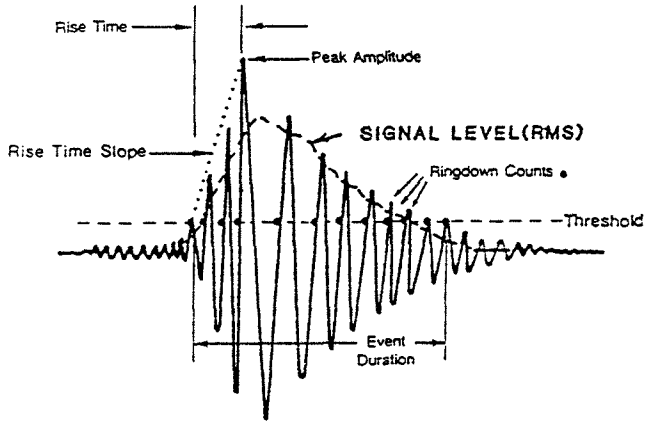

⊕ - Threshold Crossings

- First threshold crossing of a burst = event
- All threshold crossings of a burst = Ringdown Counts.

Fig. 1. Major characteristics of AE signals.

relatively well-known mechanical and electronics methods now enhanced by powerful software which effectively cleanses the AE signal.

Sources of background noise in electro-hydraulic test machines, such as that used in this investigation, are of four types. Electrical noise on the system usually is of an ampli tude of about 20 dB. Noise emanating from servo-valves and hydraulic pumps can reach a significant signal level. Noise also issues from relative movement in the load train. Under conditions of reversed cyclic loading this signal level can become very high. With the reversal of loading (stress ratio $R<0$), mechanical fretting noise increases in the specimen grips as the compression force also increases.

The latter type of noise is the hardest to eliminate. Its characteristics are very similar to those of the acoustic emission from cracks. For this reason most investigations of cyclic loading AE in the past were conducted under tension-tension loading.

Well-known mechanical and electronic filtering techniques are insufficient in the high background noise environment of the fatigue test. However, advanced techni-ques for isolating and rejecting almost all background noise are now integral to computer-controlled AE equipment. Techniques used in the present study were described by the authors in detail elsewhere[6,7]. Software-controlled AE signal-conditioning will be reviewed here briefly.

Continuous background noise due to hydraulic flows are essentially eliminated from the AE signal by a floating signal threshold, which is automatically adjusted at a 15 dB level. Extraneous signals originating outside the gage section of the test specimen are rejected with the aid of two or more AE sensors (Fig. 2), and a time-difference module (TDM). The TDM rejects unwanted signals by spatial, order-of-strike, or time-difference criteria. Further discrimination can be applied to the characteristic signal waveform (rise-rate, duration) as well as restricting data acquisition to a specific range of test parameters such as load, strain, or cycle count.

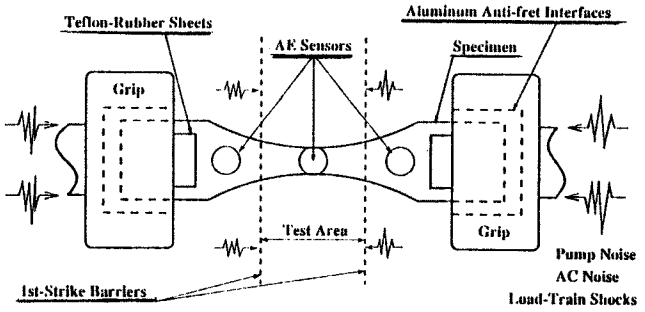

Fig. 2. Background noise elimination in materials specimen.

Experimental Procedure

Test specimens of rectangular cross-section were prepared with an hourglass test section with k_t=1.04, and minimum section of 6 mm x 7 mm. The specimens were cut radially from a new Rolls Royce turbine disk of Incoloy 901 material, in such a way that the minimum section of all specimens lay equidistant from the hub of the disk. Thus uniformity of composition, micro-structural and mechanical properties was ensured in the test section of all specimens. Material composition and mechanical properties are presented in Ref. 8. The microstructure of the material were discussed previously[8].

Static strength and fatigue tests, combined with AE monitoring, were performed at room temperature on an MTS electro-hydraulic test machine of 25 ton capacity. Axial strain was measured by fatigue-rated Kyowa foil strain-gages at the minimum section of the test specimens. Acoustic emission was monitored with a Babcock and Wilcox AET 5500 computerized system. Three 300 kHz piezoelectric sensors with 2 dB sensitivity were clamped along the gage section to constitute a linear location guarded array (Fig. 2). The preamplifiers had 60 dB gain. The signal level was further amplified in the mainframe so that the total gain of the system was 94 dB.

Following upon baseline strength and fatigue tests, a series of stress-controlled, constant amplitude fatigue tests was conducted with acoustic emission monitoring. Test frequencies were in the range 4-10 Hz, to facilitate operation of the AE sensors. In each test, the specimen was first loaded to maximum load before cycling was begun, to enable separate recording of AE due to initial dislocation dynamics and subsequent cyclic hardening softening.

Test Results

Strength Tests

For completeness, stress-strain results obtained on Incoloy 901 material at room temperature are presented in Fig. 3. Superimposed on the stress-strain curve are the acoustic emission rate (shown as raw data and a smoothed curve), as well as the integral of the AE counts.

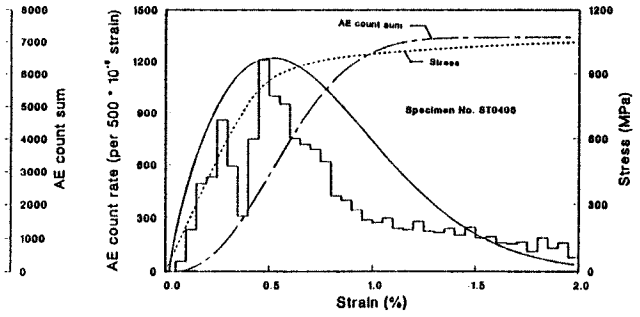

Fig. 3. Tensile stress-strain curve and AE output, Incoloy 901 at R.T.

Characteristics of Acoustic Emission During Fatigue

In spite of the large amount of disk space required

to store the data, acoustic emission was recorded throughout each load cycle, for the length of each test. The guard-array AE sensor configuration eliminated signals originating outside the specimen test section from the recorded data. Thus extraneous signals such as those emanating from load-chain noises while traversing zero load were avoided without loss of data. A complete picture of internal fatigue damage processes was obtained in the form of number of AE occurrences (events) and their intensity (ringdown counts) as a function of instantaneous stress, cycle number, and source location.

For example, the histograms in Fig. 4 present number of AE events during four tests at R=-1. The figure shows the stress- and life-dependence of physical response such as dislocation dynamics and plasticity, cyclic softening, crack initiation, crack closure, and ultimate failure. Upon initial loading considerable

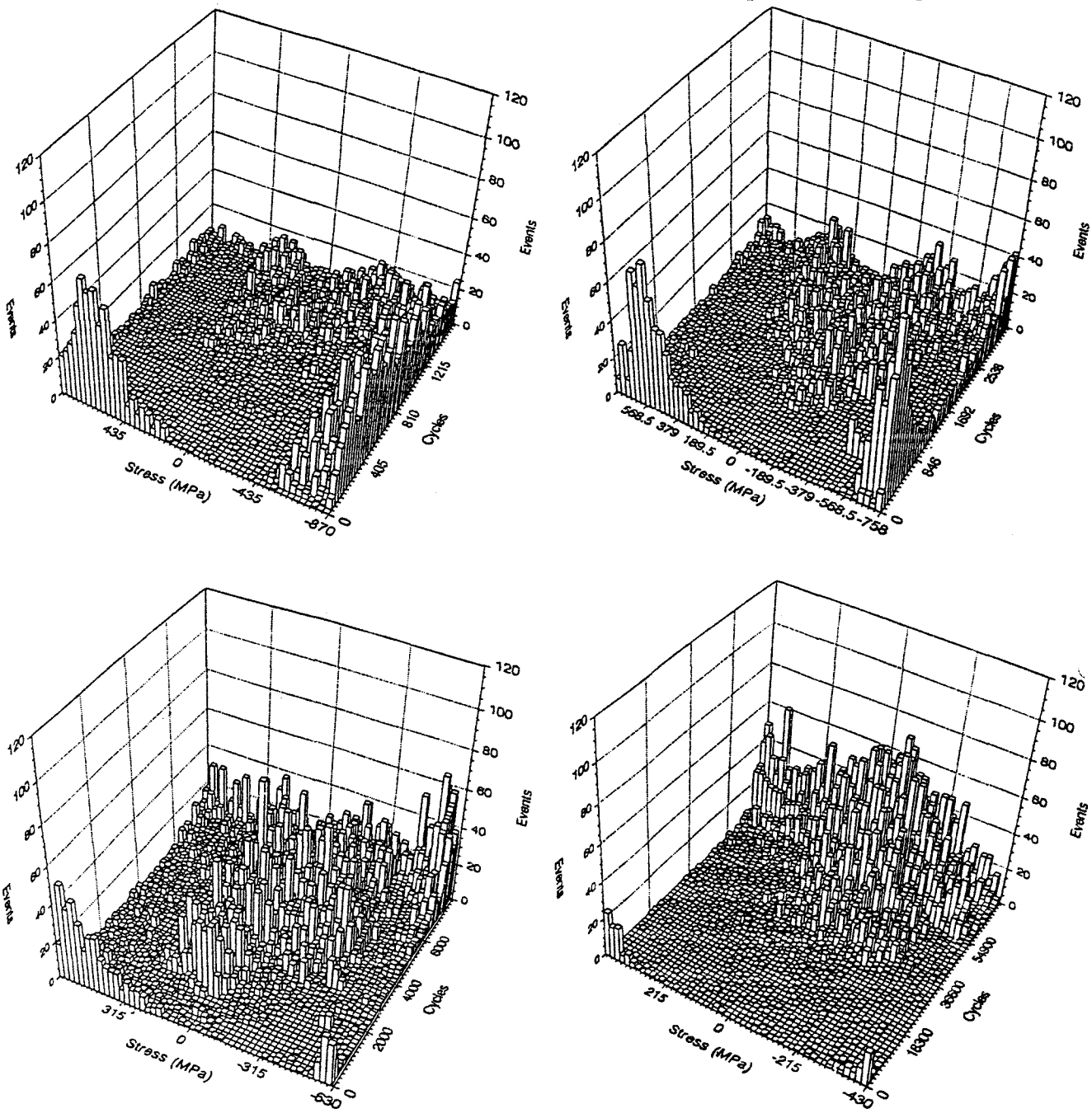

Fig. 4. Acoustic emission events during fatigue of Incoloy 901 at R=-1, showing fatigue response

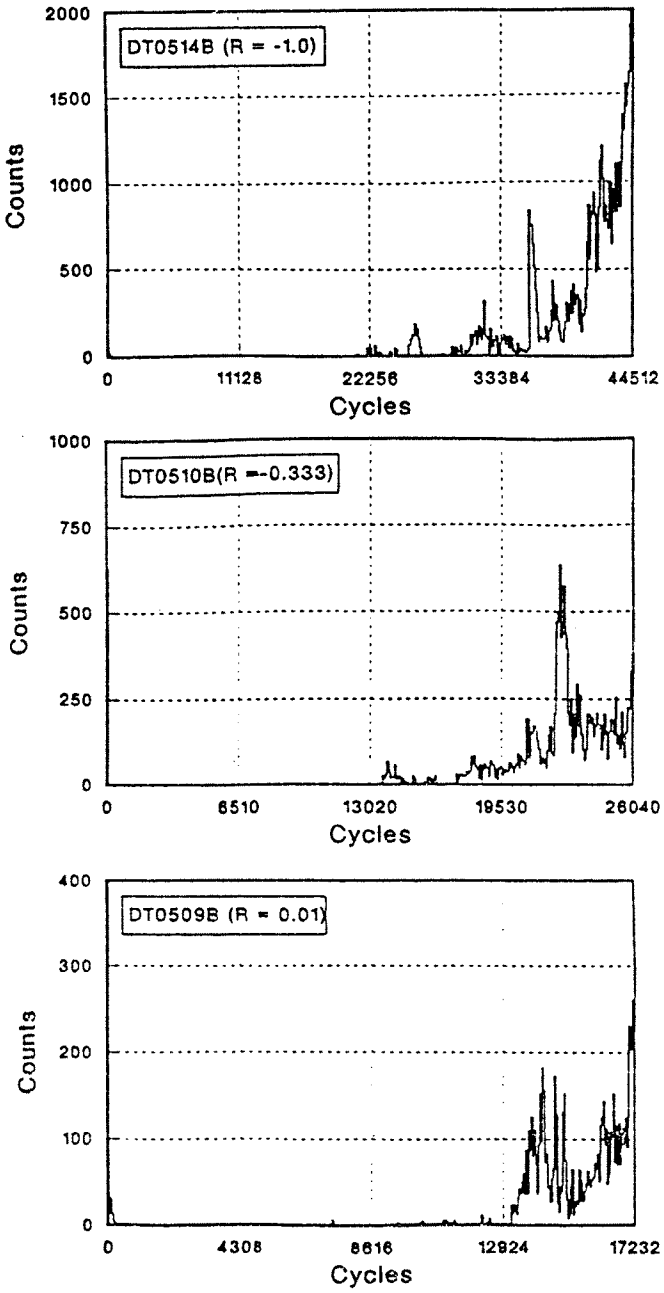

Fig. 5. AE ringdown-count rate during fatigue at $\Delta\sigma$=860 MPa.

plastic deformation due to dislocation activity at peak stresses was evident, followed by the effects of cyclic softening during the early part of each test. At higher stress amplitudes (Fig. 4a,b) AE activity continued throughout the lifetime at compressive peak stresses, but not in tension. The initiation of fatigue cracking was clearly indicated by the appearance of AE output at low stresses. Acoustic emission around zero stress was caused by crack-face grinding while the crack was closed. Thus the stress at which the crack opened/closed during each cycle was easily determined from the AE data. Just prior to fatigue failure, peak-stress plasticity was again perceived in the histograms.

Model for Fatigue Damage

Rate of acoustic emission data recorded during fatigue tests is presented in Fig. 5 in the form of ringdown counts per cycles. In general relatively intense AE activity near the start of a test was followed by a dormant period analo-gous to AE output during the post-yield strain range in stress-strain tests. Crack initiation was signaled by sudden renewal of AE output at low stresses, often with a singularly high AE peak.

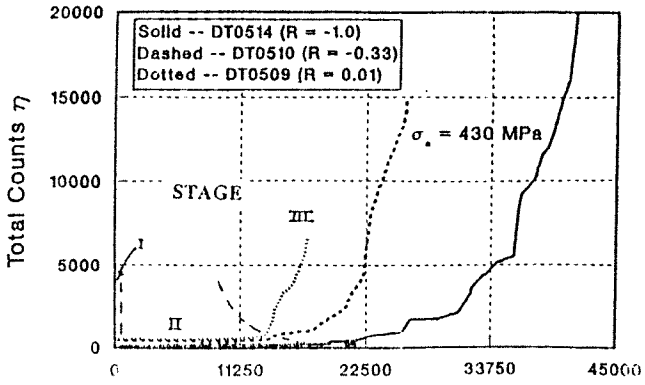

Fig. 6. AE ringdown counts during fatigue at $\Delta\sigma$=860 MPa.

Cumulative fatigue damage is revealed by integration of the ringdown counts, as shown in Fig. 6. Figure 6 was constructed using only AE data induced by plasticity at cyclic peaks, while AE output due to crack-face closure was ignored.

Three damage stages are recognizable in the integrated AE curves: (i) initial plasticity and cyclic softening, (ii) crack incubation and void-formation stage; (iii) crack propagation. By assuming a one-to-one correspondence between the sum of AE ringdown counts and fatigue damage η, the three stages indicated above were defined (Fig. 6) in the form

$$\eta = \begin{cases} c_i(\varepsilon_{max})\left\{\left[1-\exp\left[-\dfrac{(\varepsilon-\varepsilon_0)^2}{2d^2}\right]\right]\right\} + \lambda\Delta\sigma^{\alpha_n}\beta_1 & \beta_1 < 1 \quad \text{Stage I} \\ \lambda\Delta\sigma^{\alpha_n}\beta_i & \begin{cases}\beta_2 = 1 & \text{Stage II} \\ \beta_3 > 1 & \text{Stage III}\end{cases} \end{cases} \quad (1)$$

Following is an analysis of total count η variation related to the change in cyclic mechanical properties during the various stages.

Stage I - Cyclic Softening

Dislocation dynamics during the first 1/4 cycle (initial loading) caused AE output according to that shown in Fig. 3. AE events increased as load increased to maximum cyclic load. Following the initial cycle the strain amplitude in stage I increased because of cyclic softening of Incoloy 901 alloy, resulting in a high level of AE activity at compressive load peaks. Thus, the mechanisms of dislocation multiplication and cyclic softening reinforced each other to produce high level AE activity at this stage.

The total count equation can be formulated as

$$\eta_I = \eta_D + \eta_{HS} \tag{2}$$

where AE activity due to dislocations

$$\eta_D = \eta_{mxst}\left\{1-\exp\left[-\frac{(\varepsilon-\varepsilon_0)^2}{2d^2}\right]\right\} \tag{3}$$

and AE activity from cyclic hardening/softening

$$\eta_{HS} = \lambda\Delta\sigma^{\alpha}n^{\beta_1} \tag{4}$$

where ε_0 is the strain necessary to initiate AE activity, ε loading strain, η_{mxst} the total ringdown count at maximum cyclic σ_{max}, d is a scale constant and λ, α and β, empirical constants. Equation (3) reflects monotonic dislocation dynamics, and Eq. (4) corresponds to unstabilized cyclic hardening/softening, and Bauschinger effects.

Stage II - Crack Nucleation

Stage II encompasses the crack nucleation and initiation process, in which AE activity level is relatively low because of the dynamic balance between dislocation multiplication and annihilation[9,10]. During crack incubation, dislocation interactions under loading and unloading restricts dislocation motion to a steady state, and results in low AE output, as in Fig. 6. In this stage dislocation agglomeration creates microvoids in the material, which lead eventually to the formation of visible cracks.

Nevertheless, the operating deformation processes, and the resultant AE activity in stage II are strongly dependent on stress. At stress amplitudes so high that plastic strain range dominated damage advance, cyclic softening and significant dislocation motion, evidenced on the test specimens by visible slip bands, continued throughout the lifetime, and resulted in considerable AE activity even during stage II.

However, at load levels in the elastic range, AE counts increased linearly with cycles during stage II, at a rate which was constant at a given stress amplitude, as seen in Fig. 7. Regression analysis of the count rate

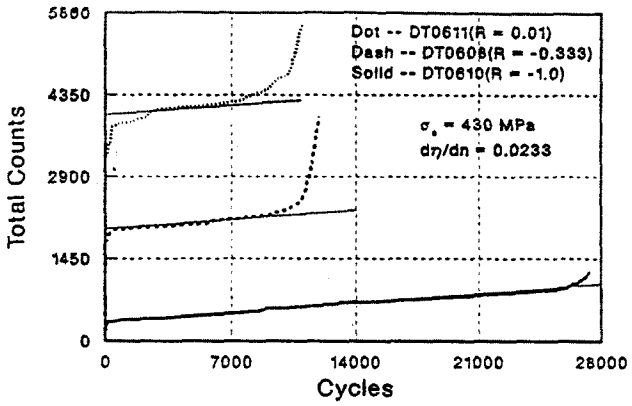

Fig. 7. AE count-sum to crack initiation, σ_a=430 MPa.

against stress amplitude in stage II resulted in α=3.1368 and λ =2.388*10^{-10} in Eq. (1), for Incoloy 901 (Fig. 8). The η_I - intercept for n=1 is shown in Fig. 9 to be a function of a stress parameter, as:

$$\eta_I = 0.069(\sigma_{max}\cdot\sigma_a/\sigma_{uts})^{1.61} \tag{7}$$

where σ_{max} is maximum stress, σ_a is stress amplitude, σ_{uts} is ultimate tensile stress for the material.

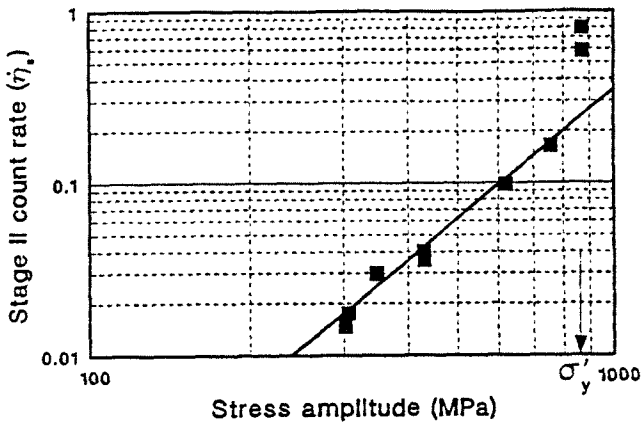

Fig. 8. Relation between stress amplitude and stage II AE count rate.

Stage III - Crack Propagation

Stage III acoustic emission began with a distinct, relatively high AE burst in the low stress region (Fig. 5), signifying initiation of a fatigue crack. A distinct advantage of the linear-location array of AE sensors used in this study was that tests could be interrupted immediately upon AE indication of fatigue crack initiation, and the crack located and measured. Microscopic examination of specimens from interrupted fatigue tests revealed initial cracks of between 50 and 100 microns in length.

After crack initiation AE output increased steadily as the crack advanced towards final failure. Much of the AE in stage III was the result of grinding of the crack faces during the low-load part of the cycle. Other sources of AE included:

i. plastic deformation in the zone in front of the crack tip, corresponding to slip bands and twinning;

ii. fracture and/or decohesion of inclusions or γ' particles;

iii. crack propagation by a) microcrack coalescence, b) transgranular cleavage, and c) intergranular fracture along twin and grain boundaries.

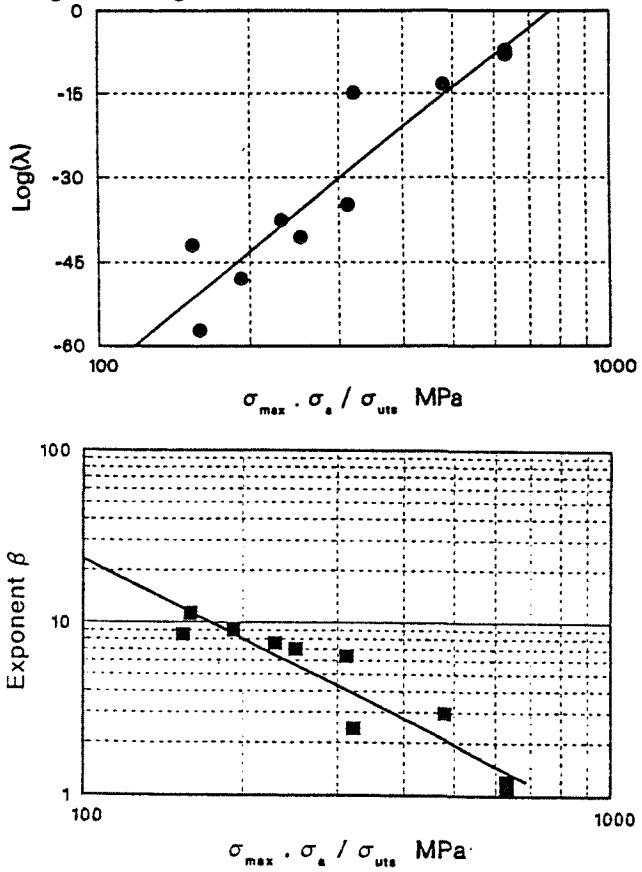

Fig. 9. Parameters λ and β as functions of stress during fatigue crack propagation.

The ringdown counts seen at any cycle n in stage III could be described by a power function (Eq. (1)), where λ and β reflect mean-stress effects (Fig. 9). Fang[11] has shown that the constants for stage III in Eq. (1) are related by a constant to the Paris relationship for crack propagation (Fig. 10).

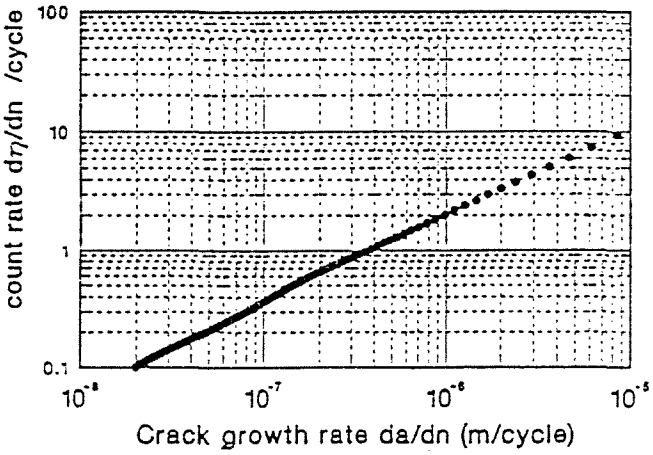

Fig. 10. Correlation between AE count-rate/cycle and crack propagation rate.

Crack Characteristics

In this section conditions for the initiation of a fatigue crack and for crack closure in smooth specimens will be examined. The determination of threshold stress intensity factor K_{th} and crack opening stress σ_{op} with the aid of AE test results will be presented.

K_{th} Determination by AE Test

Several models have been proposed to explain experimental observations or to enable theoretical evaluation of K_{th} for a given material[12-15]. However, conventional crack propagation tests do not measure the length of the incipient crack with accuracy, and require long tests to obtain a value of K_{th} at a given stress ratio, due to low crack-growth rates and large scatter. The AE technique proved to be a more convenient method of obtaining K_{th} under a given stress ratio in the fatigue test.

Several specimens were cycled at constant stress amplitudes and stress ratios, until the point of crack initiation was detected by AE peak onset as in Fig. 5. The region at which the AE peak originated on the specimen, Fig. 11, was then examined under the microscope to measure the initial crack length. K_{th} for each stress ratio was determined by expressions in Broek[16]. Excellent agreement was obtained between values of K_{th} obtained in this way with published values, at considerably reduced cost and effort (Table 2).

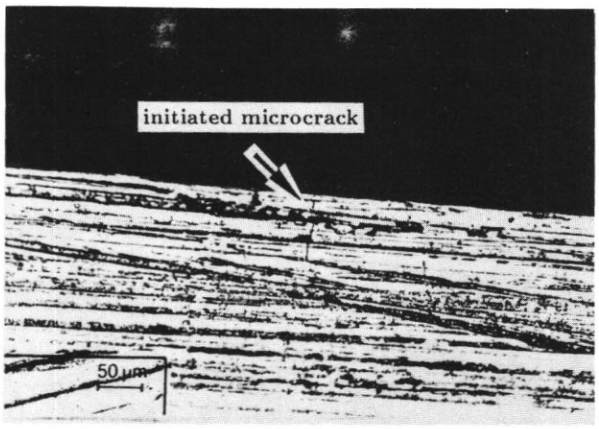

a) DTO612: R=-0.33, σ_a=430 MPa.

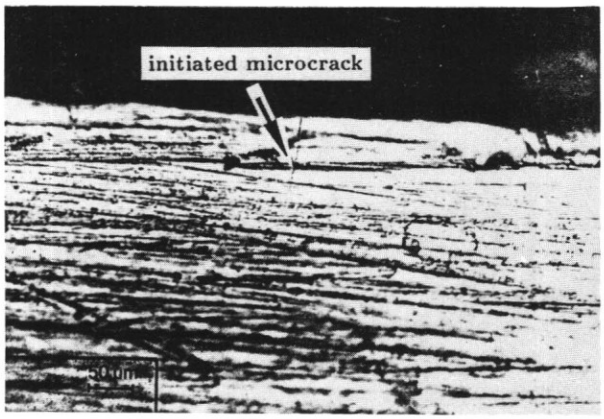

Fig. 11. Fatigue crack initiation determined by AE peak onset (untreated surface, X400).

Crack Closure

Since the AE technique is sensitive to frictional processes, it is an excellent tool for monitoring crack-face grinding during the portion of the cycle when the crack is closed. By estimating the crack-opening/closing stress from AE signatures such as shown in Fig. 4, equations in the literature for crack-opening stress were compared and ranked. For the data in Table 3 the best fit was obtained with an equation proposed by Schijve[17], but this fit could be improved further by slight modification of the first term, so that

$$\frac{\sigma_{op}}{\sigma_{max}} = 0.5 + 0.2\,R + 0.25\,R^2 + 0.1\,R^3 \qquad (2)$$

where σ_{op} and σ_{max} are crack-opening stress and maximum cyclic stress respectively.

The data used were for stress ratios between -1.0 and 0.2. For a more thorough evaluation of the various formulae, data from a wider range of stress ratios are needed. Nevertheless, the results demonstrate that AE testing is a powerful technique for studying crack closure processes during fatigue cycling.

Assessment of Fatigue Damage Accumulation

The acoustic emission ringdown count was assumed to be proportional to the number of mobile dislocations or fracturing inclusions in the material, and thus sensitive to the damage advance. For this reason total ringdown count was taken as a direct parameter reflecting the microstructural dynamics of the material[18]. A damage parameter ω was defined as the ratio of total ringdown counts η at a given instant to the sum of ringdown counts occurring until failure η_f:

$$\omega = \eta / \eta_f \qquad (3)$$

The characteristics of damage parameter ω can be understood from the experimental results appearing in Fig. 12, obtained from a monotonic strength test.

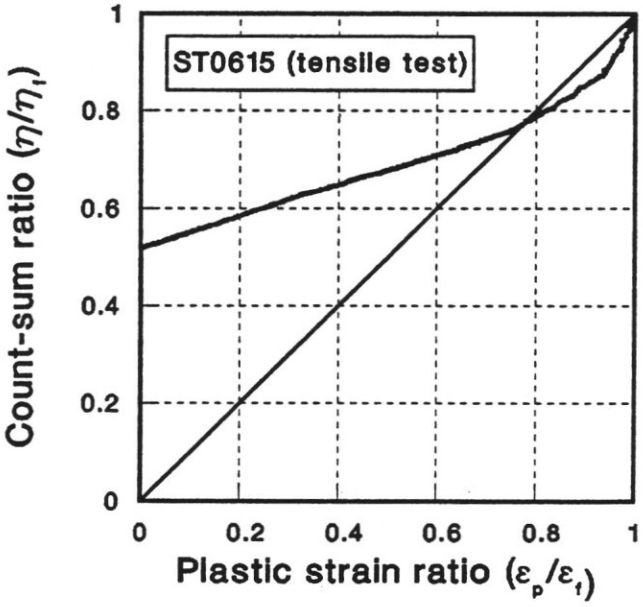

Fig. 12. Dependence of AE count-sum ratio on plastic strain in strength test.

Damage is plotted against the plastic strain to failure strain ratio, $\varepsilon_p/\varepsilon_f$. Clearly, although the rate of plastic strain was fairly con-stant throughout the test after yielding occurred, the rate of damage accumulation was not. The damage rate was high during initial yielding and crack propagation, lower in the strain-hardening regime. Thus, acoustic emission evidently reports damage processes which may themselves not be linear functions of plastic strain.

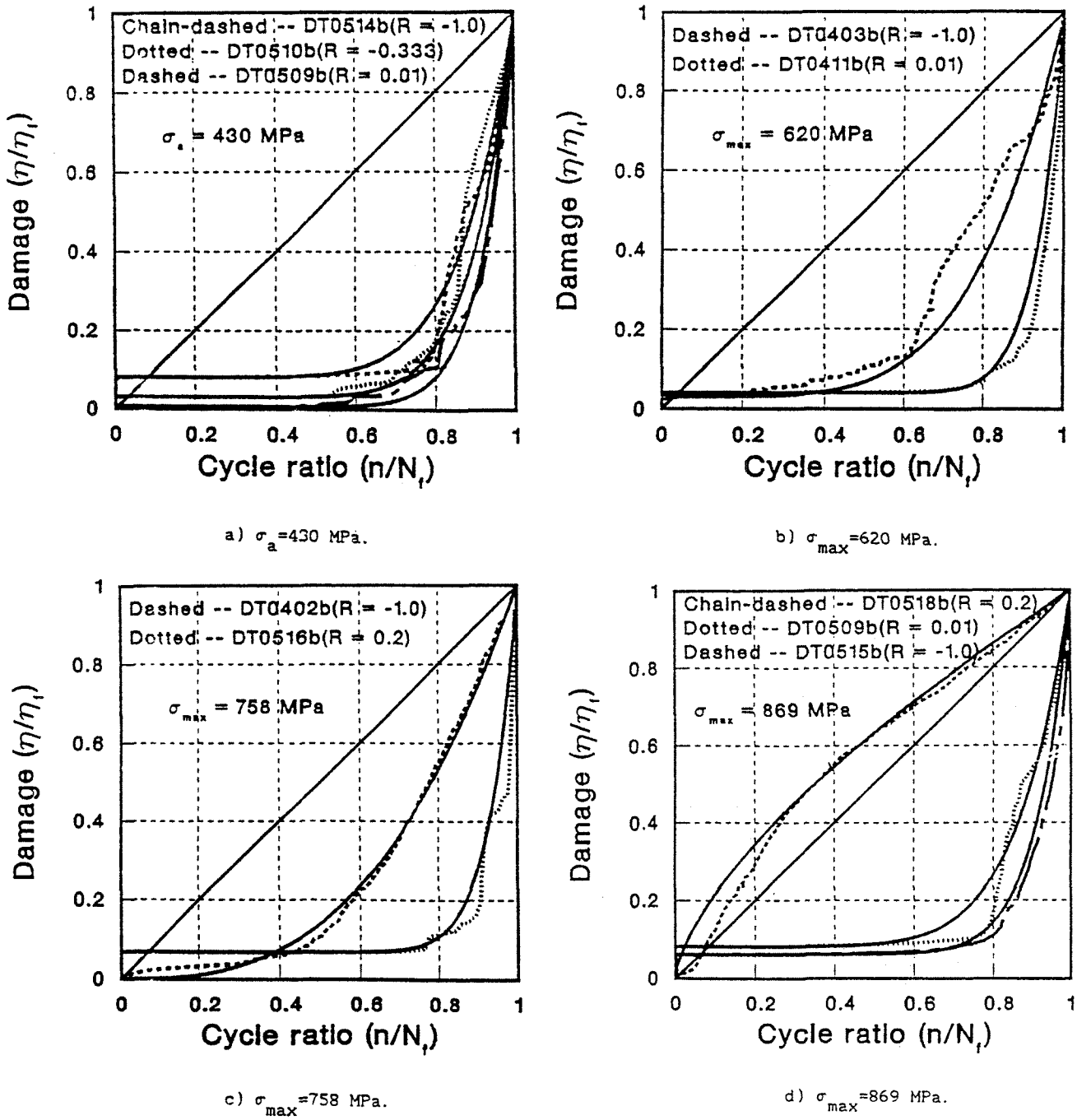

Fig. 13. Dependence of AE count-sum ratio on fatigue life.

The response of AE damage parameter ω during fatigue is plotted in Fig. 13 against cycle ratio n/N_f. Although the rate of cyclic stressing was constant throughout each test, the rate of damage accumulation was not. The damage rate was higher during initial cycling (stage I) and crack propagation (stage III), lower in the crack incubation regime (stage II). Thus, acoustic emission evidently reports damage processes which may themselves not be linear functions of stress, strain or time.

Note that the damage plotted in Fig. 13 is only that recorded at tensile and compressive load peaks. AE output emanating from crack-face grinding was not considered as due to fatigue damage, since it occurred primarily behind the crack tip. Initial plasticity and cyclic softening (stage I), crack incubation and initiation (stage II), and finally crack propagation (stage III), are clearly evident in the figure. The solid curves

superimposed on the experimental results represent calculations made using a model devised for predicting fatigue damage throughout the entire lifetime.

Based on these figures, a model for damage accumulation was proposed as shown in Fig. 14. The

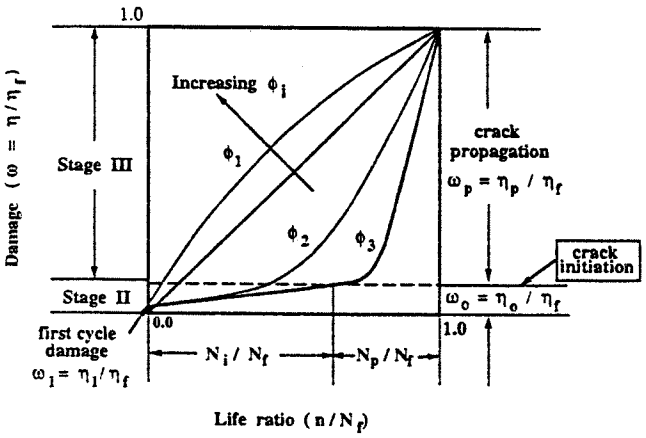

Fig. 14. Schematic of nonlinear damage as a function of load parameter ϕ.

basic assumption in Fig. 14 is that the relative increase of ringdown counts $d\eta/\eta$ is a linear function of the relative increase of cycles, dn/n. That is,

$$\frac{d\eta}{\eta} = \psi(\phi_i, \delta_i)\frac{dn}{n} \qquad (4)$$

where δ_i are material constants, and ϕ_i are a function of load. The function $\psi(\phi_i,\delta_i)$ is positive for any ϕ_i and δ_i since the cyclic damage process and corresponding acoustic emission are considered irreversible. Under given loading conditions, ϕ and consequently $\psi(\phi,\delta)$, are constant.

Integrating Eq. (4) and introducing boundary conditions, the damage equation is obtained:

$$\omega = \omega_1 + (1-\omega_1)\left(\frac{n}{N_f}\right)^{\psi(\phi,\delta)} \qquad (5)$$

Since the failure lifetime can be expressed as

$$N_f = g(\phi_i,\delta_i) = g(\Delta\sigma,\sigma_m,R,\delta_i) \qquad (6)$$

the monotonically varying ψ a function of N_f A preliminary suggestion for function ψ might be:

$$\psi = C(N_f)^{\alpha} \qquad (7)$$

which, when combined with the function for C postulated by Manson and Halford [19]

$$C = N_{ref}^{\gamma} \qquad \gamma = 0.4 \sim 0.5 \qquad (8)$$

leads to an expression for damage:

$$\omega = \omega_1 + (1-\omega_1)\left(\frac{n}{N_f}\right)^{\left(\frac{N_f}{N_{ref}}\right)^{0.45}} \qquad (9)$$

The solid curves in Fig. 13, calculated from Eq. (9), fit the experimental damage curves well. The transition fatigue life N_t was selected as the reference life N_{ref} in Eq. (9), equal to 200 in the present investigation (except for one specimen for which the stress amplitude was on the order of the yield stress, where N_{ref} =4000).

In its present form, the damage relation, Eq. (9), refers to life parameter N_f only. It does not refer directly to loading parameters. Work is continuing in order to relate the damage function with the cyclic loading parameters.

Conclusions

Test results demonstrated that acoustic emission technique can be applied to gain understanding of the variables which control time- and stress-dependent fatigue damage processes in materials. Computerization of AE test techniques permitted reliable AE measurements under cyclic loading at arbitrary stress ratios, including fully-reversed loading. Fatigue damage accumulation was evaluated in real time on smooth Incoloy 901 specimens, in terms of an AE definition of damage, and a damage function was developed.

The AE technique revealed the occurrence of crack closure, and crack-opening closing stress was clearly indicated by the AE signature. Dislocation dynamics related to cyclic softening were proposed in explanation of AE occurring during the compressive half of early load cycles. Mechanisms of fatigue microcrack initiation were examined. The threshold stress intensity factor value determined by AE tests for crack initiation points was found to be comparable with that obtained from conventional crack propagation tests. However, K_{th} was obtained by AE method at much less time and cost. Three stages of the fatigue damage process were identified by their AE signature, and formulated as a damage relation in terms of total AE ringdown counts. This formulation has yet to be developed further, in terms of the fatigue loading parameters. To this end further endeavor is required in order to achieve a more complete data set. Such work includes: wider range of stress-ratio; complementary

study of cyclic-hardening material; program loading; fatigue investigation with the aid of AE techniques at elevated temperature; studies of small cracks.

Acknowledgment

This work was supported by Rolls Royce plc, Derby, UK, under the guidance of Dr. Leon Grabowski, monitor.

References

1. Mastor, I.I. and Gradov, O.M., 1986, *Int. J. of Fatigue*, Vol. 8, No. 2, pp. 67-71.
2. Kohn, D.H. and Ducheyne, P., 1992, *J. of Mat. Sci.*, Vol. 27, pp. 1633-1641.
3. Berkovits, A. and Fang, D., 1992, "Acoustic Emission as a Measure of Fatigue Damage", in *Durability of Metal Aircraft Structures*, S.N. Atluri et al., eds., Atlanta Technology Publs., Atlanta, GA, pp. 38-46.
4. Berkovits, A. and Fang, D., 1993, "An Empirical Design Model for Fatigue Damage on the Basis of Acoustic Emission Measurements", in *Durability and Structural Reliability of Airframes*, A.F. Blom, ed., Proc. 17th ICAF Symp., Stockholm, EMAS Publ., England.
5. ASTM, 1982, "Definition of Terms Relating to Acoustic Emission", ASTM Standard E610-82.
6. Fang, D. and Berkovits, A., 1993, "Fatigue Damage Mechanisms on the Basis of Acoustic Emission Measurements", in *Novel Experimental Techniques in Fracture Mechanics*, A. Shukla, ed., ASME Publ. AMD, Vol. 176, pp. 219-236.
7. Fang, D. and Berkovits, A., 1994, "Acoustic Emission Techniques in Fatigue Testing of Metal Alloys", to be published in *Experimental Techniques*.
8. Berkovits, A. and Fang, D., 1992, "Modelling Fatigue Damage Accumulation in Nickel Base Superalloys", Semi-Annual Report III, Faculty of Aerospace Eng., Technion, ASL No. 142.
9. Mughrabi, H., Wang, R., Differt, K. and Essmann, U., 1993, "Fatigue Crack Initiation by Cyclic Slip Irreversibilities in High-Cycle Fatigue", *Fatigue Mechanisms*, ASTM STP 811, pp. 5-45.
10. Morris, E.F., 1980, *Met. Trans. A.*, Vol. 11A, pp. 365-379.
11. Fang, D., 1993, "Micro- and Macro-Evaluation of Fatigue Damage Accumulation", D.Sc. Dissertation, Technion-Israel Inst. Tech., Haifa, Israel.
12. Minakawa, K. and McEvily, A.J., 1981, *Scripta. Met.*, Vol. 15, pp. 633-636.
13. Wanhill, R.J.H., 1988, *Eng. Frac. Mechanics*, Vol. 30, No. 2, pp. 233-260.
14. Cooke, R.J. and Beevers, C.J., 1974, *Mat. Sci. Eng.*, Vol. 13, pp. 201-210.
15. Masounave, J. and Bailon, J.P., 1975, *Scripta Met.*, Vol. 9, pp. 723-730.
16. Broek, D., 1986, *Elementary Engineering Fracture Mechanics*, 4th ed., Martinus Nijhoff Publ., Dordrecht.
17. Schijve, J., 1976, "The Stress Ratio Effect on Fatigue Crack Growth in 2024-T3 Alclad and the Relation to Crack Closure", Delft University of Technology, Memorandum M-336.
18. Heiple, C.R. and Carpenter, S.H., 1983, "acoustic Emission from Dislocation Motion", in *Acoustic Emission*, J.R. Mathews, ed., Gordon and Breach Publ., New York, pp. 33-54.
19. Manson, S.S. and Halford, G.R., 1986, *Eng. Frac. Mechanics*, Vol. 25, No. 5-6, pp. 539-571.

Specimen	Crack length (μm)	Location on test section (mm)	Surface	ΔK_{th} (MN.m$^{-3/2}$)	R_σ	σ_{max} (MPa)	σ_a (MPa)	N_o
DTO611	33.0	34	front	9.8	0.01	869	430	11,664
	55.6	32	rear	12.3				
DTO612	58.3	16	front	9.3	-0.33	645	430	12,360
	72.2	17	rear	10.9				
DTO610	86.8	37	front	8.0	-1.0	430	430	27,664
	75.2	40	rear	7.4				
DTO608	66.7	38	front	10.5	-0.33	645	430	11,640
	-	-	-	-				
DTO614	111.1	43	front	13.0	-1.0	620	620	2,256
	116.7	44	rear	13.3				
Rolls Royce Data	-	-	-	10.0	0.1	-	-	-
				5.8	0.8			

Table 2 K_{th} for Incoloy 901 at Room Temp.

Specimen	Stress ratio R	Experiment $\frac{\sigma_{op}}{\sigma_{max}}$	Experiment σ_{op} (MPa)	Schijve (1976) $\frac{\sigma_{op}}{\sigma_{max}}$	Schijve (1976) σ_{op} (MPa)	Modified $\frac{\sigma_{op}}{\sigma_{max}}$	Modified σ_{op} (MPa)
DTO403	-1.0	0.435	270	0.400	248	0.450	279
DTO411	0.01	0.516	320	0.452	280	0.502	311
DTO402	-1.0	0.439	333	0.400	303	0.450	341
DTO516	0.2	0.612	464	0.501	380	0.550	417
DTO415	-1.0	0.472	410	0.400	348	0.450	391
DTO515	-1.0	0.489	425	0.400	348	0.450	391
DTO509	0.01	0.400	348	0.452	393	0.502	436
DTO518	0.2	0.570	496	0.501	435	0.550	478
DTO510	-0.33	0.420	271	0.407	262	0.457	295
DTO514	-1.0	0.477	205	0.400	172	0.450	202
DTO605	-1.0	0.453	195	0.400	172	0.450	202
Average Error				0.018		0.009	
Standard Deviation				6.8		5.6	

Table 3 Crack opening stress.